

We are IntechOpen, the world's leading publisher of Open Access books Built by scientists, for scientists

6,900

Open access books available

186,000

International authors and editors

200M

Downloads

Our authors are among the

154

Countries delivered to

TOP 1%

most cited scientists

12.2%

Contributors from top 500 universities



WEB OF SCIENCE™

Selection of our books indexed in the Book Citation Index
in Web of Science™ Core Collection (BKCI)

Interested in publishing with us?
Contact book.department@intechopen.com

Numbers displayed above are based on latest data collected.
For more information visit www.intechopen.com



Crack Growth in AlCu4Mg1 Alloy under Combined Cyclic Bending and Torsion

Dariusz Rozumek and Ewald Macha
Opole University of Technology
Poland

1. Introduction

Aluminium and its alloys are the materials tested for many years and frequently used for the elements of fatigue loading. The most characteristic properties of aluminum are low weight (3 times less than iron) and low melting point (about 2.5 times smaller than the iron). In addition, aluminum has good corrosion resistance properties by creating a thin and tight (passive) layer of Al_2O_3 . Therefore, aluminum alloys are widely used in the construction of airplanes, vehicles, transport equipment, machinery or parts of building structures. All technical alloys are divided into two groups: alloys for plastic working and foundry alloys. The boundary between them is determined by the maximum content of an additional component dissolved in the solid solution at the eutectic temperature. The appearing eutectic adversely affects the technological properties of the alloy (reduced susceptibility to plastic working). As for aluminum alloys subjected to plastic working and heat treatment in order to their hardening, duralumin is most widely applied. These alloys are usually subjected to heat treatment consisting of annealing, saturating or ageing. In the paper (Kocańda & Kozubowski, 1974) the authors studied the influence of microstructure on the alloy PA6 on appearance of fatigue microcracks. It was noted the presence of gas microbubbles, and precipitations of secondary phases. It was found that gas microbubbles are the source of fatigue microcracks. Döring et al. (2006) presented the test results described by the ΔJ -integral range, obtained under non-proportional loading including the crack closure. The test results obtained under tension with torsion for three materials (two steels and one aluminium alloy) were analysed. Different loading paths were applied (circle, ellipse, octant, square and cross). Fatigue crack growth behavior (Chung & Yang, 2003) in Al 6061-T6 thick aluminium plate with composite material patch was studied. Five inclined crack plates repaired with patch were tested. Crack branching at the threshold level and crack closing can be described (Pokluda, 2004) with the local approach including the ratio of the grain size to the plastic zone size. At that level of the crack development there are three mixed-cracking modes before the crack front, even in the case of mode I only, visible outside the tested element. Three materials were tested (steel, aluminium alloy and titanium alloy). The aim of this chapter is the presentation of static and cyclic properties of aluminum alloy AlCu4Mg1 and to present the test results of fatigue crack growth in plane notched specimens under bending and proportional bending with torsion.

2. Experimental procedure

2.1 Material and specimens

AlCu4Mg1 aluminium alloy included in the standard EN AW- 2024 and PN-92/H-93667 was subjected to tests. The tested material belongs to a group of medium-alloy duralumins. Beams of such a shape are used, among others, as torsion bars in cars (Renault), trucks and tanks (attachment of springs), and intermediate beams for gas and oil wells. The AlCu4Mg1 aluminium alloys with copper and magnesium, i.e. duralumin, belong to the alloys of high strength properties. They contain a solid solution α and numerous precipitations of phases Al_3Mg_2 , CuAl_2 and triple S-phase (Al_2CuMg), and dark precipitations of the phase containing Fe: $\text{Fe}_3\text{Si}_2\text{Al}_{12}$, occurring mainly at grain boundaries of phase α . Precipitations of these phases strongly influence strength and hardness of AlCu4Mg1 alloy, especially precipitations at the phase boundaries reduce plastic properties. Cracks of the specimens made of aluminium alloys of phase α structure occur on the slip plane $\{111\}$ under the shear stress independent on spatial orientation of the grain. Figure 1 shows a microstructure of AlCu4Mg1 aluminium alloy that consists of lighter α grains with darker phases CuAl_2 and Al_2CuMg . The microstructure is characterized by a bands grains according to the plastic treatment direction: elongated grains of the phase α are to 50 μm in width and the minor phase CuAl_2 and Al_2CuMg diameter from 5 to 10 μm .

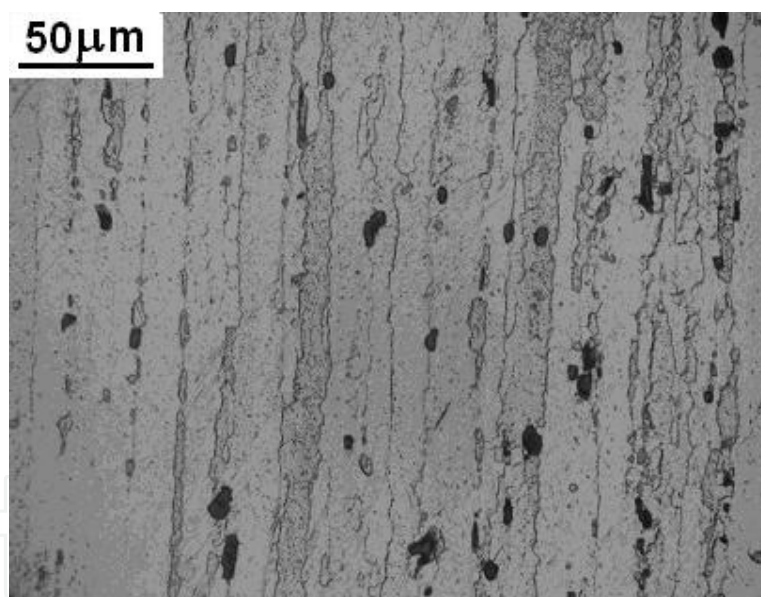


Fig. 1. Microstructure of AlCu4Mg1 aluminium alloy, magnification 500x

Specimens with rectangular cross-sections for bending (area 60 mm²) and bending with torsion (area 64 mm²) and dimensions: length $l = 110$ (90) mm, height $w = 16$ (10) mm and thickness $g = 4$ (8) mm were tested (see Fig. 2). Each specimen had an external unilateral notch with depth 2 mm and radius $\rho = 0.2$ mm. The notches in the specimens were cut with a milling cutter and their surfaces were polished after grinding. Chemical composition and some mechanical properties of the tested aluminium alloy are given in Tables 1 and 2.

The critical value of the integral for AlCu4Mg1 aluminium alloy is $J_{Ic} = 0.026$ MPa·m (ASTM E1820-99). Strain-based fatigue curves are shown in Fig. 3, where elastic and plastic components are given too. As usual, such curves have been described by a linear law in a

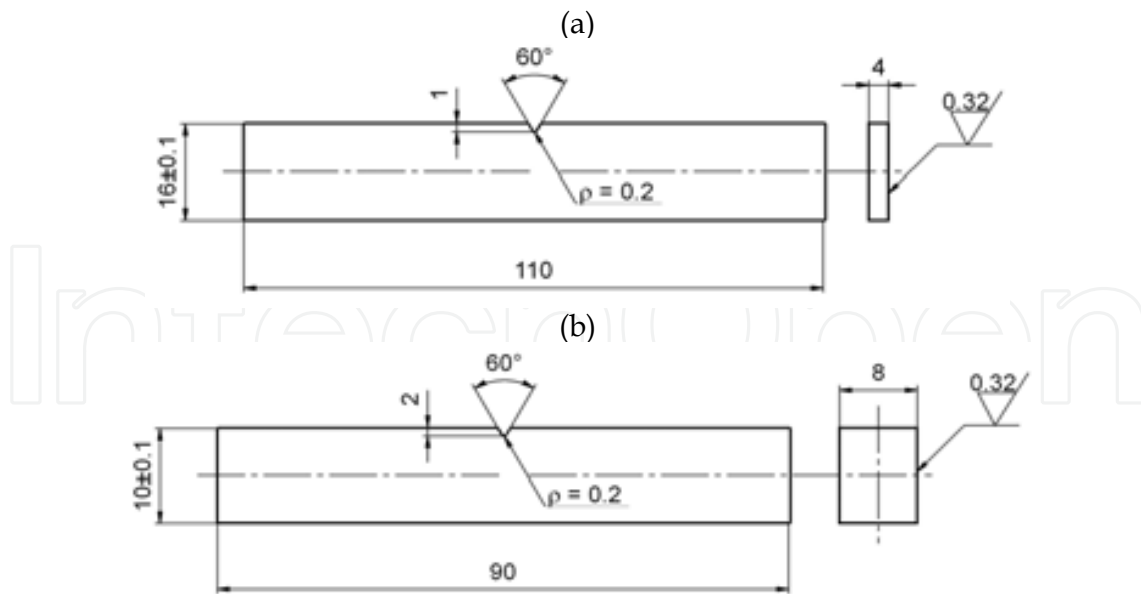


Fig. 2. Shape and dimensions of specimen, dimensions in mm for: (a) bending, (b) bending with torsion

Cu	Mn	Zn	Mg	Fe	Cr	Si	Ti	Al
4.15	0.65	0.50	0.69	0.70	0.10	0.45	0.20	bal.

Table 1. Chemical composition of the AlCu4Mg1 aluminium alloy (in wt %)

σ_y MPa	σ_u MPa	E GPa	ν
382	480	72	0.32

Table 2. Monotonic quasi-static tension properties of the AlCu4Mg1 aluminium alloy

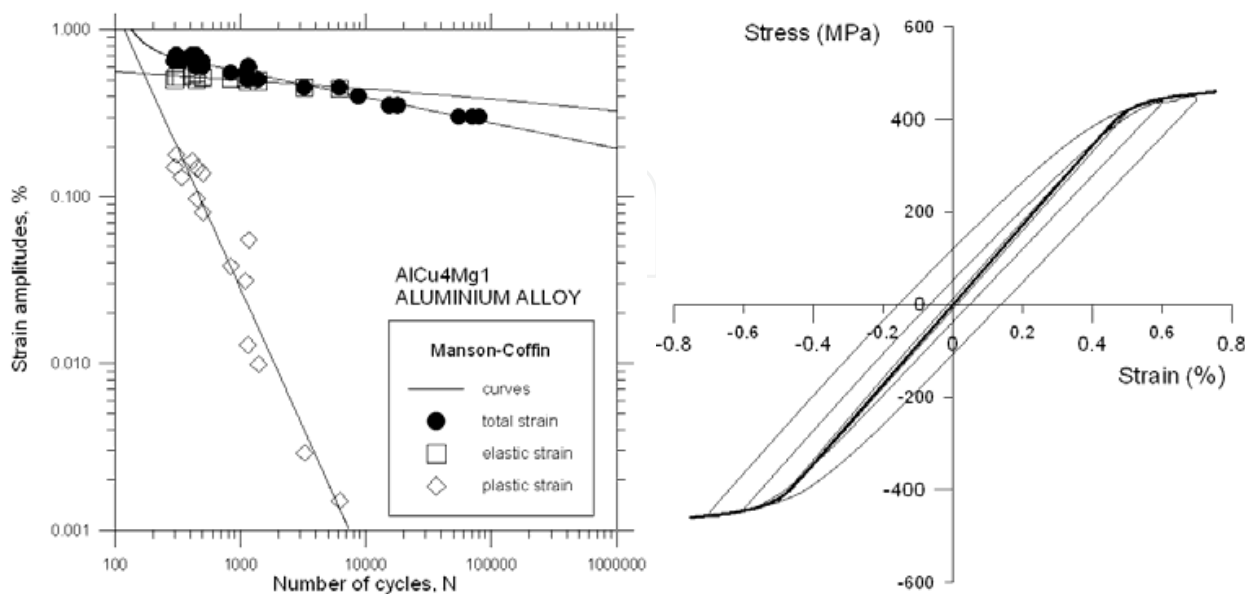


Fig. 3. Fatigue curves under strain control and some stabilized hysteresis loops of AlCu4Mg1 aluminium alloy

log-log diagram, as suggested by the Manson-Coffin model. In the same figures, some stabilised hysteresis loops are displayed too. Coefficients of the Ramberg-Osgood equation describing the cyclic stress curve under tension-compression conditions with $R = -1$ for AlCu4Mg1 aluminium alloy are the following (Rozumek, 2005): the cyclic strength coefficient K' , the cyclic strain hardening exponent n' , fatigue strength coefficient σ'_f , fatigue ductility coefficient ϵ'_f , fatigue strength exponent b , fatigue ductility exponent c (Table 3). After the analysis of axial cyclic stress-strain curves, it was concluded that AlCu4Mg1 aluminium alloy is cyclically hardening material during fatigue tests.

The static and cyclic properties for AlCu4Mg1 aluminium alloy were obtained from the tests done at the laboratory of Department of Mechanics and Machine Design, Opole University of Technology, Poland.

K' MPa	n'	σ'_f MPa	ϵ'_f	b	c
563	0.033	605	0.105	-0.051	-0.858

Table 3. Fatigue properties of the AlCu4Mg1 aluminium alloy

2.2 Fatigue testing

Fatigue tests were performed in the low cycle fatigue (LCF) and high cycle fatigue regimes (HCF) under the load ratio $R = M_{\min} / M_{\max} = -1, -0.5, 0$. The tests were carried out under controlled loading from the crack occurrence to the specimen fracture. Starting point of crack initiation at notch root was observed on side of the specimen. The tests were performed on a fatigue test stand MZGS-100 (Rozumek & Macha, 2006) where the ratio of torsion moment to bending moment was $M_T(t) / M_B(t) = \tan\alpha$, where $\alpha = 30^\circ, 45^\circ$ and 60° (Fig. 4) and loading frequency was 29 Hz. The total moment $\bar{M}(t) = \bar{M}_T(t) + \bar{M}_B(t)$ was

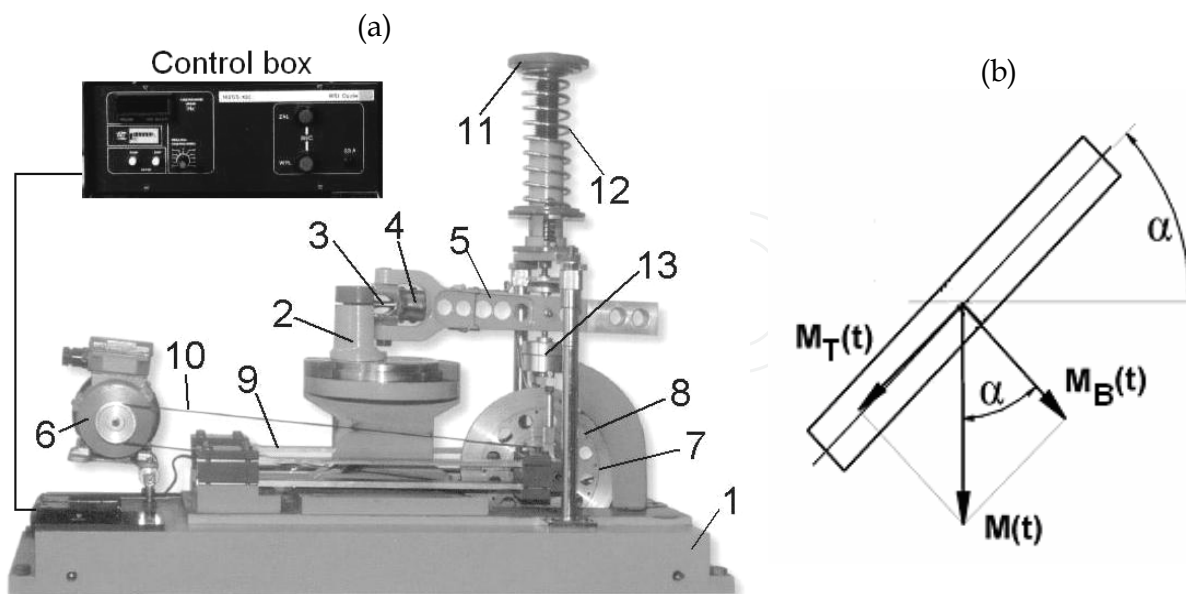


Fig. 4. Fatigue test stand MZGS-100 (a) and loading of the specimen (b) where: 1 - bed, 2 - rotational head with a holder, 3 - specimen, 4 - holder, 5 - lever (effective length = 0.2 m), 6 - motor, 7 - rotating disk, 8 - unbalanced mass, 9 - flat springs, 10 - driving belt, 11 - spring actuator, 12 - spring, 13 - hydraulic connector.

generated by forces on the arms 0.2 m in length. When $\alpha = 0^\circ$ we have pure bending; for $\alpha = 90^\circ$ we obtain pure torsion. Shearing force on a fatigue test stand MZGS-100 coming from bending takes very small values, below 2% of the maximum moment. The fatigue test stand MZGS-100 (Fig. 4a) consist of power unit, control unit and loading unit. Loading unit consists of cyclic and static loading. Cyclic loading is obtained by vertical movements of the lever. Static loading is obtained by a spring pressure. Crack development was observed on the specimen surface with the optical method. The fatigue crack increments were measured with a digital micrometer located in the portable microscope with magnification of 25 times and accuracy of 0.01 mm. At the same time, a number of loading cycles N was written down. Under bending with torsion, dimension "a" of the crack growth was defined as increments of length and angle α_1 (Fig. 12) of the crack measured on the specimen side surface.

2.3 Microstructure and fatigue crack path in AlCu4Mg1

Fig. 5 shows the surface of the specimen made of AlCu4Mg1 aluminium alloy, tested under loading $M_a = 15.6 \text{ N}\cdot\text{m}$ corresponding to the nominal stress amplitude to the crack initiation $\sigma_a = 104 \text{ MPa}$ and the stress ratio $R = -0.5$ after $N_f = 49000$ cycles. Different magnifications were selected in such a way that they present a path of the main crack, about 3 mm in length. Fig. 5b presents the final history of the crack about $250 \mu\text{m}$ in length, cut off from Fig. 5a and magnified in order to analyse the crack development. In AlCu4Mg1 aluminium alloy transcrystalline microcracks can be seen in grains of phase α , in the axial section of the specimen (see Fig. 5b). The main characteristics of long cracks development is their regularity of propagation and orientation. There are no short cracks, some or several μm in length, deflecting from the main crack, which we can observe, for example, in titanium alloys.

The forming faults from the main crack can be seen, which run according to directions of phases Al_2CuMg (almost perpendicularly to the loading applied), and next they go into the phase α . On the fractures we can observe usually transcrystalline cracks through grains of the phase α , but also cracks along the grain boundaries can be noticed. The main cracks developed on the planes of maximum shear stresses. In the considered material we have mixed cracking, i.e. brittle and plastic. In Fig. 5b we can observe both kinds of cracking near the main crack, i.e. pits of different size, typical for plastic cracking, and cracks along the grain boundaries typical for brittle fractures.

2.4 Stress distribution

If the specimen is both bended by moment M_B and twisted by moment M_T (Fig. 4b), then in a given rectangular cross-section normal stresses form under the influence of bending and the shear stresses result from torsion (Rozumek & Macha, 2009). The normal stresses change from zero in the neutral axis to the maximum value $\sigma_a = \frac{6M_B}{gw^2}$ in the extreme fibres (σ_{\max})

(Fig. 6). Shear stresses occur changing from zero in the specimen axis to the maximum value

$$\tau_a = \frac{M_T}{k_1 w g^2} \quad (k_1 = 0.208 - \text{ratio of the height to the thickness of specimen}) \text{ in the most distant}$$

points of specimen's shorter side (τ_{\max}) (Fig. 6).

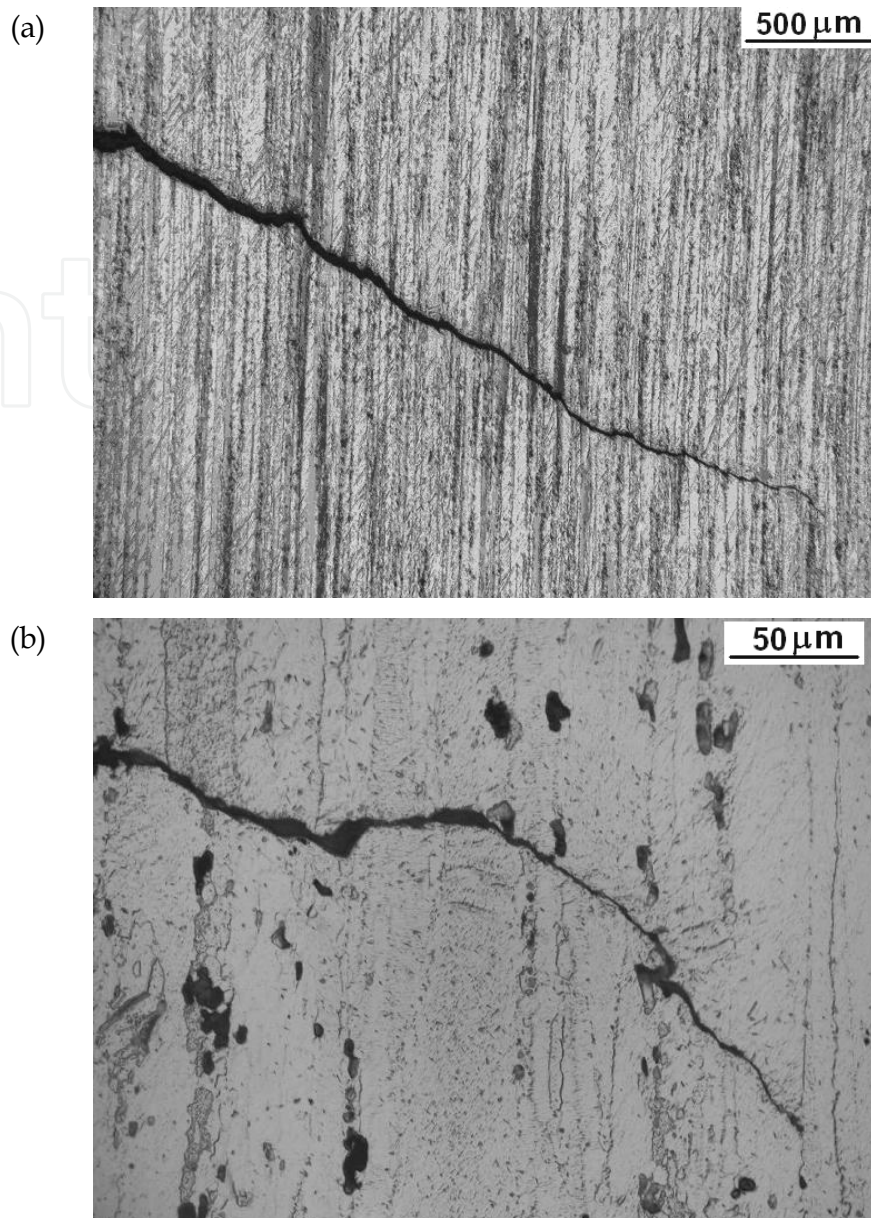


Fig. 5. The fatigue crack path in the AlCu4Mg1 under bending: (a) magnification 50x, (b) magnification 500x

De Saint-Venant worked on the problem of stress distribution under torsion. He found that stresses were equal to zero inside and in the corners of the bar, and they were the biggest in the centers of square sides (longer sides of the rectangle). In the specimen under torsion, cross-sections do not remain plane but are subjected to deformation or the so-called deplanation. If torsion is unfree (as in the presented case), then shear and normal stresses occur induced by torsion. In the presented case, the normal stresses were about three times bigger than shear stresses (due to the occurrence of the notch in the plane of their action). Under simultaneous action of the two moments, M_B and M_T , the most dangerous stress state forms in the planes most distant from both the neutral axes of the specimen (Fig. 6 - σ_{\max}). The stress intensity factors can be expressed as: for mode I, $K_I = Y_I \sigma_a \sqrt{\pi a}$ and for mode III, $K_{III} = Y_3 \tau_a \sqrt{\pi a}$.

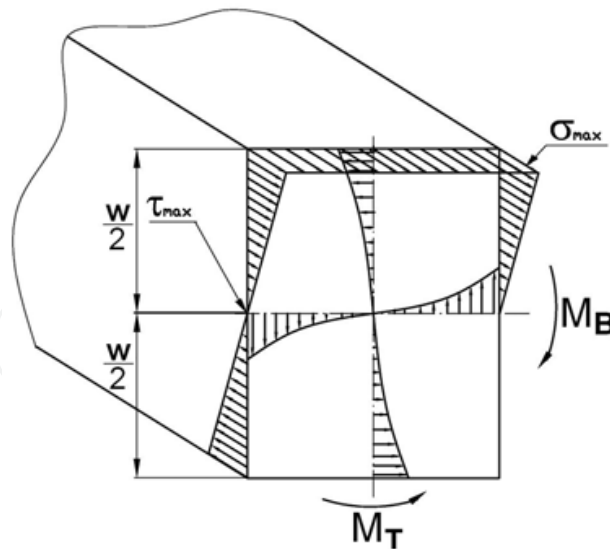


Fig. 6. Distribution of normal and shear stresses in the specimen subjected to bending with torsion (Rozumek & Marciniak, 2010)

2.5 ΔJ parameter criterion

In the case of mixed mode I and III, the range of the equivalent parameter ΔJ was assumed as the sum of ΔJ_I and ΔJ_{III}

$$\Delta J = \Delta J_{eq} = \Delta J_I + \Delta J_{III} . \quad (1)$$

The ΔJ -integral range for mode I and mode III is calculated from (Rozumek, 2005)

$$\Delta J_I = (1 - \nu^2) \Delta K_I^2 / E + \pi Y_1^2 a (\Delta \sigma \Delta \epsilon_p / \sqrt{n'}) , \quad (2)$$

$$\Delta J_{III} = (1 + \nu) \Delta K_{III}^2 / E + \pi Y_3^2 a (\Delta \tau \Delta \gamma_p / \sqrt{n'}) , \quad (3)$$

where the first term of Eqs. (2) and (3) concerns the linear-elastic range, and the other term refers to the elastic-plastic range, a - crack length, E - Young's modulus, ν - Poisson's ratio, $\Delta \sigma$, $\Delta \tau$ - ranges of stresses under bending and torsion in the near crack tip, respectively, $\Delta \epsilon_p$, $\Delta \gamma_p$ - ranges of plastic strains under bending and torsion in the near crack tip, respectively.

The stress intensity factors ranges ΔK_I for mode I and ΔK_{III} for mode III were calculated from

$$\Delta K_I = Y_1 \Delta \sigma \cos^2 \alpha \sqrt{\pi a} , \quad (4)$$

$$\Delta K_{III} = Y_3 \Delta \sigma \sin \alpha \cos \alpha \sqrt{\pi a} , \quad (5)$$

according to (Harris, 1967) and (Chell & Girvan, 1978), for mode I and mode III the correction coefficients are

$$Y_1(a/w) = 5 / \sqrt{20 - 13(a/w) - 7(a/w)^2} , \quad (6)$$

$$Y_3(a/w) = \sqrt{(2w/a) \tan(\pi a / (2w))} . \quad (7)$$

3. Experimental results and discussion

3.1 Finite and boundary element model

Stresses and strains in the elastic-plastic ranges were calculated with use of the finite element method (FRANC2D software) for bending and the boundary element method (FRANC3D software) for bending with torsion. A specimen model was built and divided into finite elements with the use of CASCA graphic processor, which was integrated with FRANC2D software. Each of these areas was covered with a net of finite elements. Fig. 7a shows the division of the area around the crack into finite elements. In the model, six-nodal triangular elements were applied; the triangles were of different dimensions. The geometrical model of the specimen was created using OSM software, with the boundary element mesh generated in the FRANC3D software. The programs include the nonlinear physical Ramberg-Osgood curve of cyclic strain of the material tested. It was decided that calculations would be based on incremental elastic-plastic analysis including the kinematic model of material hardening. Having made the specimen outline, segments were divided and closed areas were defined. A boundary element mesh was put on each area. The programs design the mesh automatically. The calculations were performed for a two-dimensional and three-dimensional models of the notched specimens. Figure 7b shows division of the notch region into boundary elements. The model shown in Fig. 7b includes ten-node elements being tetrahedral (the model including 1354 triangular elements). Loading values assumed for calculations were the same as those applied in the experiments. Magnitude and shapes of boundary elements depend on division of intervals closing a given area. The greatest mesh concentration occurs in the area of the crack development (Fig. 7).

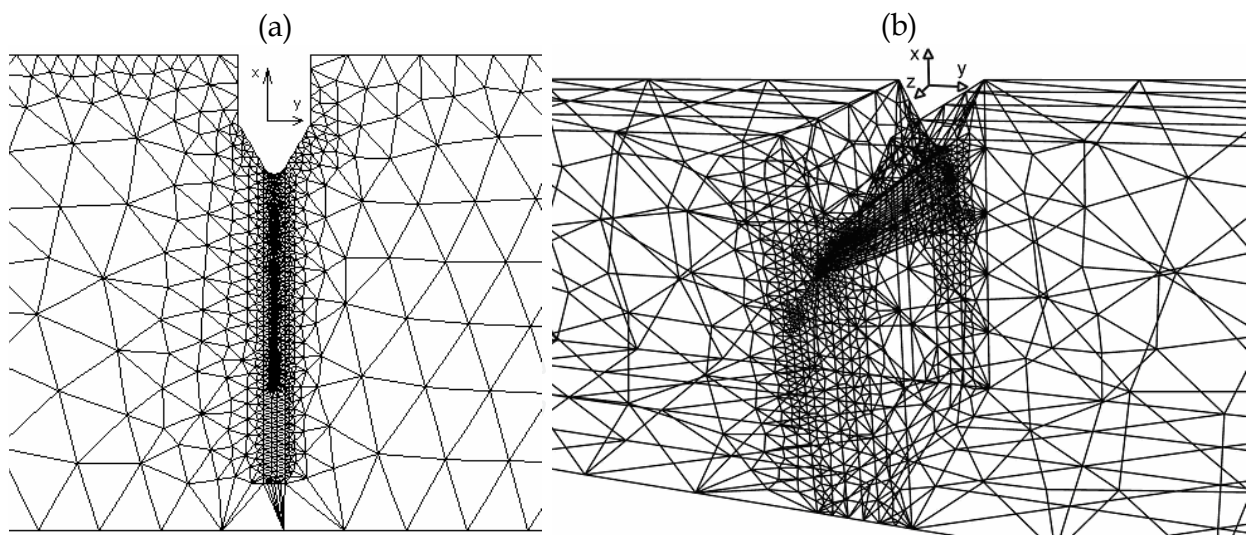


Fig. 7. Division of the notch region into finite and boundary elements in the software (a) FRANC2D, (b) FRANC3D

Next, one end of the specimen is restrained (thus taking away the degrees of freedom from the nodes of specimen model) and it is fixed in direction of axes x , y and z . In order to perform numerical calculations, it is necessary to introduce material data (such as the yield point, Young's modulus, Poisson's ratio, temperature, material density, critical value - for example, J_{Ic} integral) into the FRANC3D software.

3.2 Bending

Each series of specimens made of AlCu4Mg1 aluminium alloy was subjected to cyclic bending by the constant amplitude moment $M_a = 15.64 \text{ N}\cdot\text{m}$ (which corresponded to the nominal amplitude of normal stresses $\sigma_a = 104 \text{ MPa}$ before the crack initiation) and different load ratio $R = -1, -0.5, 0$ (different mean bending moment $M_m = 0, 5.21, 15.64 \text{ N}\cdot\text{m}$). The test results were shown as graphs of the crack length "a" versus the number of cycles N and crack growth rate da/dN versus the ΔJ parameter. ΔJ was compared with the ΔK stress intensity factor range. The theoretical stress concentration factor in the specimen $K_t = 4.29$, was estimated with use of the model (Thum et al., 1960). From the fatigue crack length "a" versus number of cycles N curves reported in Fig. 8, it appears that after changing the load ratio R from -1 to 0, fatigue life decreases. The tests were conducted under constant amplitude loading for three different values M_{max} . During the tests the lengths of fatigue cracks were measured and the current number of cycles was recorded. Basing on these measurements graphs were made "a" versus number of cycles N, which were used for calculating the fatigue crack growth rate. Graphs of the fatigue crack growth rate da/dN versus ΔJ parameter for the material tested under three load ratios R are shown on a binary logarithmic system in Fig. 9.

The test results presented in Fig. 9 were approximated with the empirical formula (Rozumek, 2005)

$$\frac{da}{dN} = \frac{B \left(\frac{\Delta J}{J_0} \right)^n}{(1-R)^2 J_{Ic} - \Delta J}, \quad (8)$$

where $\Delta J = J(\Delta\sigma)$ - range of J parameter, B and n - coefficients determined experimentally, R - load ratio, $J_0 = 1 \text{ MPa}\cdot\text{m}$ - per unit value introduced to simplify the confounded coefficient unit B.

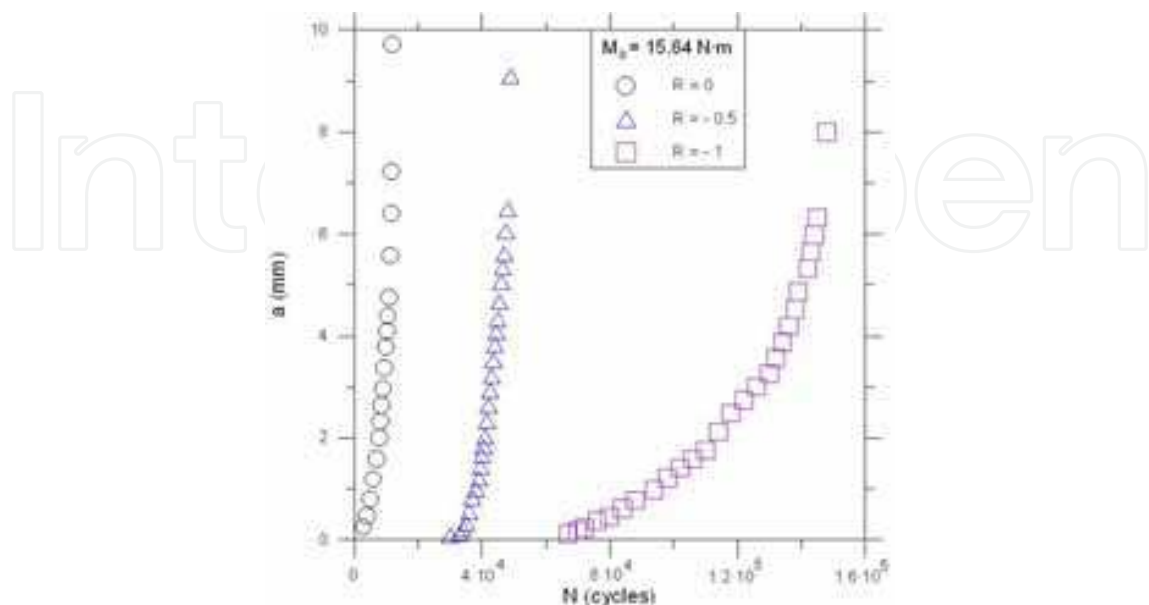


Fig. 8. Fatigue crack length versus number of cycles under bending

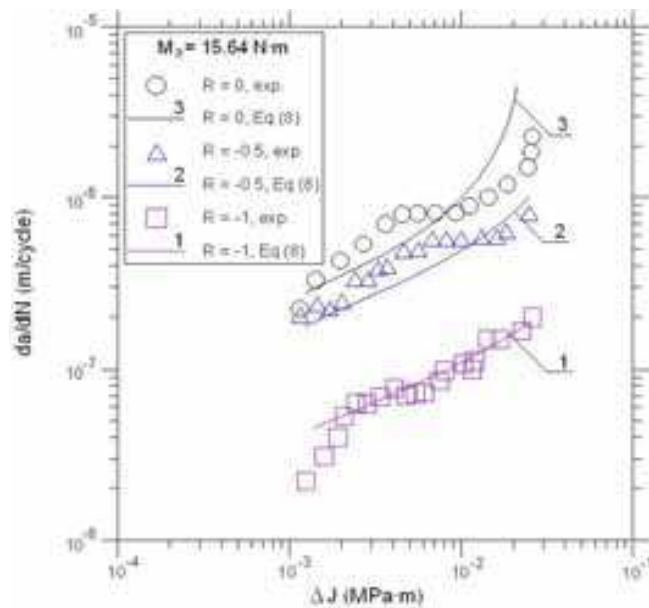


Fig. 9. Comparison of the experimental results with calculated ones according to Eq. (8)

It has been observed that in Fig. 9 (graphs 1, 2, 3), the change of the load ratio R from -1 to 0 is accompanied by an increase in the fatigue crack growth rate. From the graphs it appears Fig. 9 that influence of the loading mean value on the crack growth rate in the AlCu4Mg1 alloy is significant. For example, from Fig. 9 it appears that while changing the value of the load ratio from $R = -1$ to $R = 0$, a nine fold increase in fatigue crack growth rate has been noticed for $\Delta J = 3 \cdot 10^{-3}$ MPa·m. The empirical coefficients B and n occurring in Eq. (8) were calculated with the least square method and they were shown in Table 4. It means that B and n are not dependent on a kind of the material only. The test results for cyclic bending include the error not exceeding 20% at the significance level $\alpha = 0.05$ for the correlation coefficients r_w given in Table 4. The correlation coefficients take high values in all the considered cases and it means that there is a significant correlation of the test results and the assumed empirical formula (8). Table 4 also contains coefficients of the multiple correlation r_w applied in Eq. (8) and expressed by equation (Rozumek & Macha, 2006)

$$r_w = \sqrt{\frac{r_{y1}^2 + r_{y2}^2 - 2r_{y1}r_{y2}r_{12}}{1 - r_{12}^2}}, \quad (9)$$

where r_{12} , r_{y1} , r_{y2} – coefficients of cross correlation.

Fig.	Graphs	B MPa·m ² /cycle	n	r_w
9	1	$1.04 \cdot 10^{-7}$	0.51	0.96
9	2	$9.49 \cdot 10^{-8}$	0.28	0.97
9	3	$8.11 \cdot 10^{-8}$	0.30	0.94

Table 4. Coefficients B and n in Eq. (8) and correlation coefficients r_w for the curves shown in Fig. 9

Calculating ΔJ parameter, we can find that there is a functional relation between the loading range, the elastic-plastic strain range, the crack tip opening displacement and the crack length. High values of correlation coefficients show that all these factors were approximately included. Above a certain value of ΔJ parameter, the fatigue crack growth rate increases rapidly without further increase of loading. Such behaviour is connected with an unstable crack growth rate in the final stage of specimen life. In this period the stress drop can be observed as plasticization increases. Application of the ΔJ parameter is reasonable in the case of elastic-plastic materials and those with yield stress. An analysis of correlation of ΔJ and ΔK parameters was carried out to show that the ΔJ parameter is more advisable than ΔK . Therefore the following equation was used:

$$\Delta J^* = \frac{\Delta K^2}{E}, \quad (10)$$

where stress intensity factor range ΔK calculated from $\Delta K = K_{\max} - K_{\min} = Y_1 \Delta \sigma \sqrt{\pi a}$ and $\Delta \sigma = \sigma_{\max} - \sigma_{\min}$ stress range and $\Delta \sigma = 2\sigma$ for $R = -1$, Y_1 - correction coefficient including finite of the specimen dimensions for mode I applied in Eq. (6).

In the linearly-elastic range, the ΔJ^* parameter calculated from Eq. (10) were compared with the results obtained from tests. The relative error was below 5%. Figure 10 shows the relation between the parameters ΔJ^* and ΔJ for three load ratios R . A good linear relation (in the double logarithmic system) between these two parameters in the case of the fatigue crack growth rate for the tested material was observed. In the AlCu4Mg1 alloy and bending, this occurs for $\Delta J < 4 \cdot 10^{-3}$ MP·m (Fig. 10). This means that in this test range under controlled loading, the parameter ΔJ plays a similar role to the parameter ΔK up to the moment when plastic strain occurs. When plastic strains increase, we can find an increasing difference between ΔJ^* and ΔJ . The difference results from the fact that the parameter ΔJ^* does not include plastic strains. At the final stage of specimen life, when ΔJ parameter approaches the

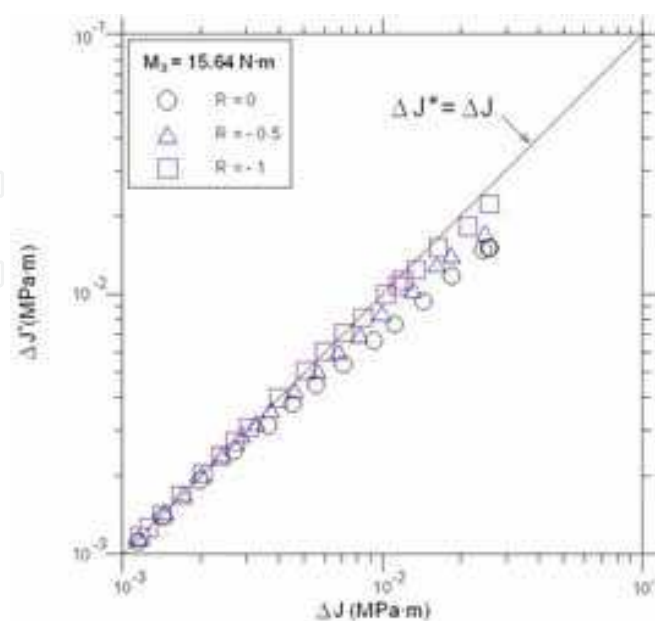


Fig. 10. The relationship between ΔJ^* and ΔJ for bending

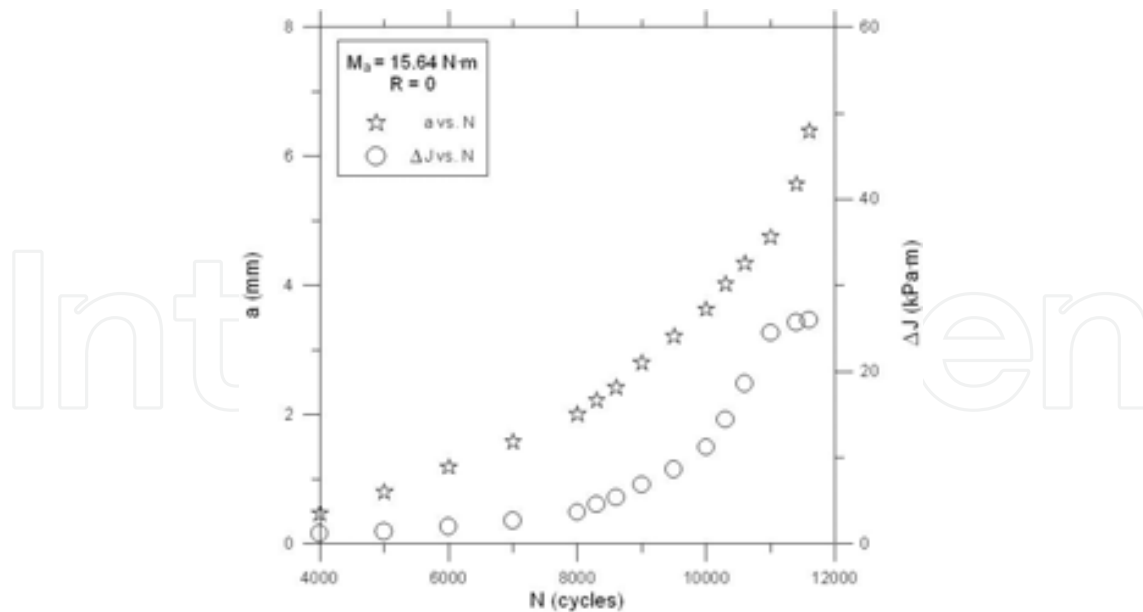


Fig. 11. Variation with cycles of crack length and ΔJ for bending and $R = 0$

critical value of J_{IC} , the crack growth rate increases rapidly (Fig. 10, $R = 0$) and leads to the material failure. For example in Fig. 11 (AlCu4Mg1 aluminium alloy and $R = 0$) fatigue crack growth “a” versus the number of cycles N and ΔJ parameter versus the number of cycles N are shown in the linear system. In this figure we can observe fatigue crack growth since the beginning of the propagation until the specimen failure. In Fig. 11 the graph ΔJ versus N also shows that ΔJ parameter increases with the number of cycles until reaching 11000 cycles, then the graph stabilises (it becomes almost constant).

3.3 Bending with torsion

The chapter contains the fatigue crack growth test results obtained under proportional bending with torsion (Rozumek, 2009). The tests were performed on a fatigue test stand MZGS-100 (Fig. 4a), where the ratio of torsion moment to bending moment was $M_T(t)/M_B(t) = \tan\alpha$, where $\alpha = 30^\circ, 45^\circ$ and 60° (Fig. 4b). Unilaterally restrained specimens were subjected to cyclic bending with torsion (mixed mode I+III) with the constant amplitude of moment $M_a = 7.92$ N·m and load ratio $R = M_{\min} / M_{\max} = -1, -0.5, 0$ (for three different values $M_{\max} = 7.92, 10.56, 15.84$ N·m), which corresponded to the nominal amplitude of normal stresses $\sigma_a = 80.36, 65.63$ and 46.41 MPa ($\sigma_{\max} = K_t\sigma_a = 302.15, 246.77, 174.50$ MPa) and the nominal amplitude of shear stresses $\tau_a = 37.18, 52.58$ and 64.39 MPa before the crack initiation. The theoretical stress concentration factor in the specimen under bending $K_t = 3.76$, was estimated with use of the model (Thum et al., 1960). During experimental tests fatigue cracks lengths and angles α_1 (Fig. 12) were measured and number of cycles were registered. Next, on the basis of experimental results in the range of linear-elastic, the range of ΔK parameter was analytically calculated for mode I and mode III loading. Stresses and strains calculations in linear-elastic and elastic-plastic were made with use of numerical method (FRANC3D software). Measurement of the crack length were made on both sides of the specimens. At one side, the cracks were a little greater than at the other side. For calculations of the ΔJ parameters, greater cracks are assumed because they mainly influence the specimen failure. Also the stress fields are greater at one side of the specimen. During

the tests on the observed reproducibility of the test specimens. Fig. 12 shows an example of the crack path under proportional bending with torsion for $\alpha = 45^\circ$.

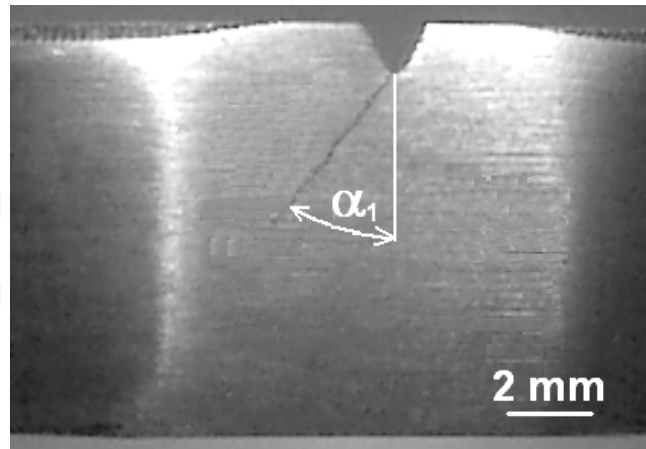


Fig. 12. Crack path in specimen under proportional bending with torsion for $R = -1$ and $\alpha = 45^\circ$

Figures 13, 14 and 15 present results of fatigue crack length versus the number of cycles for mixed mode I+III and $\alpha = 30^\circ, 45^\circ$ and 60° , respectively.

From the graphs in Figs. 13, 14, 15 it appears that changes of the angle α from 30° to 60° are accompanied by decrease of fatigue life of the specimens for the load ratio $R = -1, -0.5, 0$, as well as after changing the load ratio from -1 to 0 , fatigue life decreases. Figures 16, 18 and 20 for load ratio $R = -1, -0.5, 0$ show fatigue crack growth rates da/dN versus ΔJ parameter for pure mode I and pure mode III and three the ratio of torsion moment to bending moment ($\alpha = 30^\circ, 45^\circ$ and 60°). The ΔJ parameter for pure mode I and pure mode III was calculated from Eqs. (2) - (7). Next, Figs. 17, 19, 21 present the results according to equation (1) for mixed mode I+III loading.

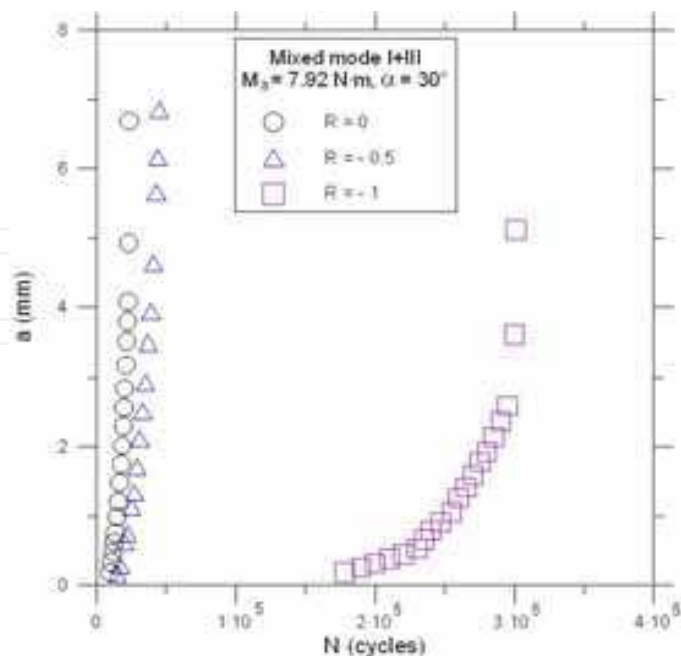


Fig. 13. Fatigue crack length versus number of cycles under mixed mode I+III loading for $\alpha = 30^\circ$

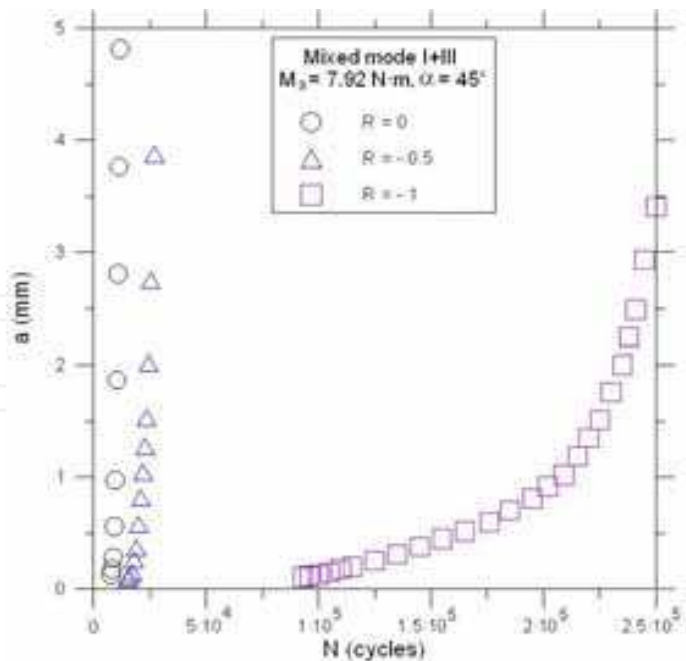


Fig. 14. Fatigue crack length versus number of cycles under mixed mode I+III loading for $\alpha = 45^\circ$

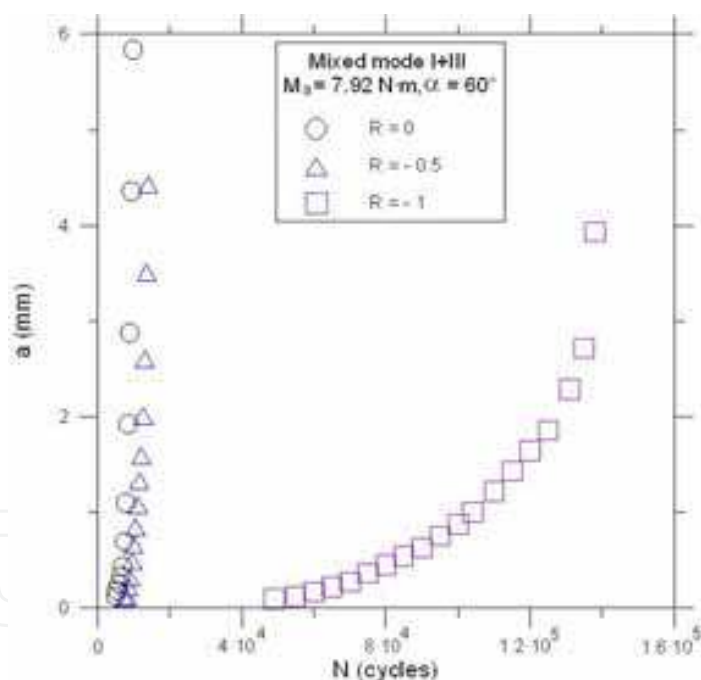


Fig. 15. Fatigue crack length versus number of cycles under mixed mode I+III loading for $\alpha = 60^\circ$

From Figs. 16 - 21 it appears that the fatigue crack growth rate increases when we increase α from 30° to 60° and load ratio R from -1 to 0 in the AlCu4Mg1 aluminium alloy. Moreover (Figs. 16, 18, 20), the fatigue crack growth rate is higher for mode III than for mode I for the same value of ΔJ and load ratio $R = -0.5, 0$. It was found that for $R = -1$ and $\alpha = 30^\circ$ (Fig. 16) the crack growth rate was higher for mode III than for mode I in the case of the same value of ΔJ ; for $R = -1$ and $\alpha = 60^\circ$ (Fig. 20) a higher rate is observed for mode I.

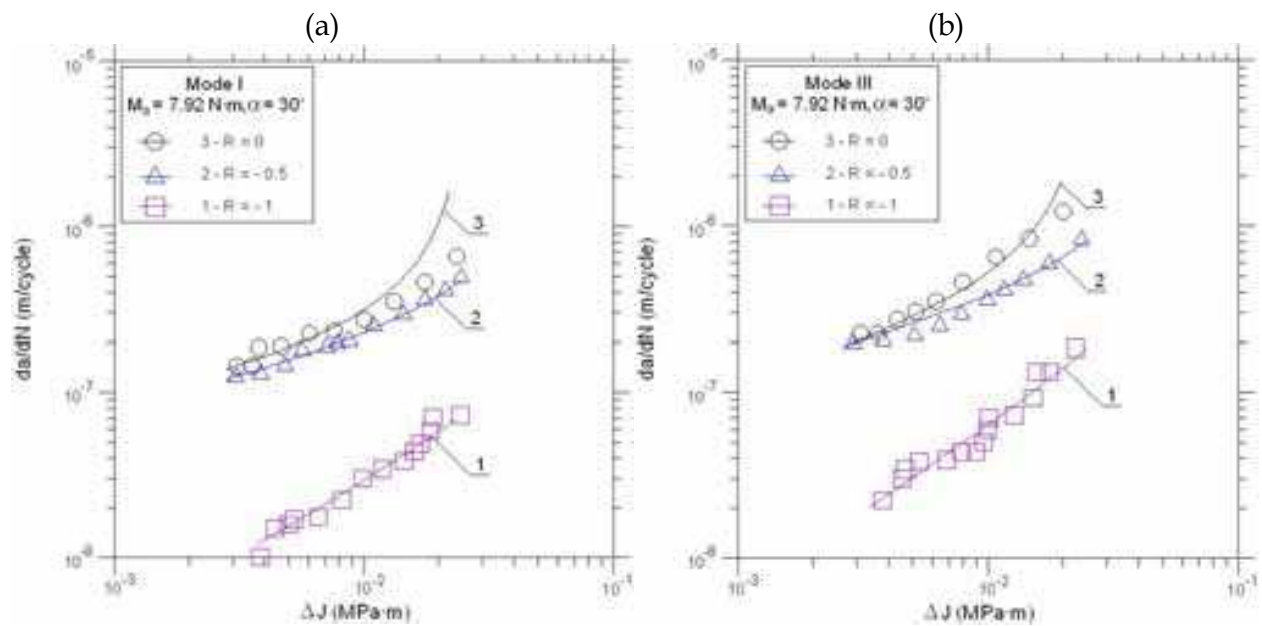


Fig. 16. Comparison of the experimental results with calculated ones according to Eq. (8) for $\alpha = 30^\circ$ and: (a) mode I, (b) mode III

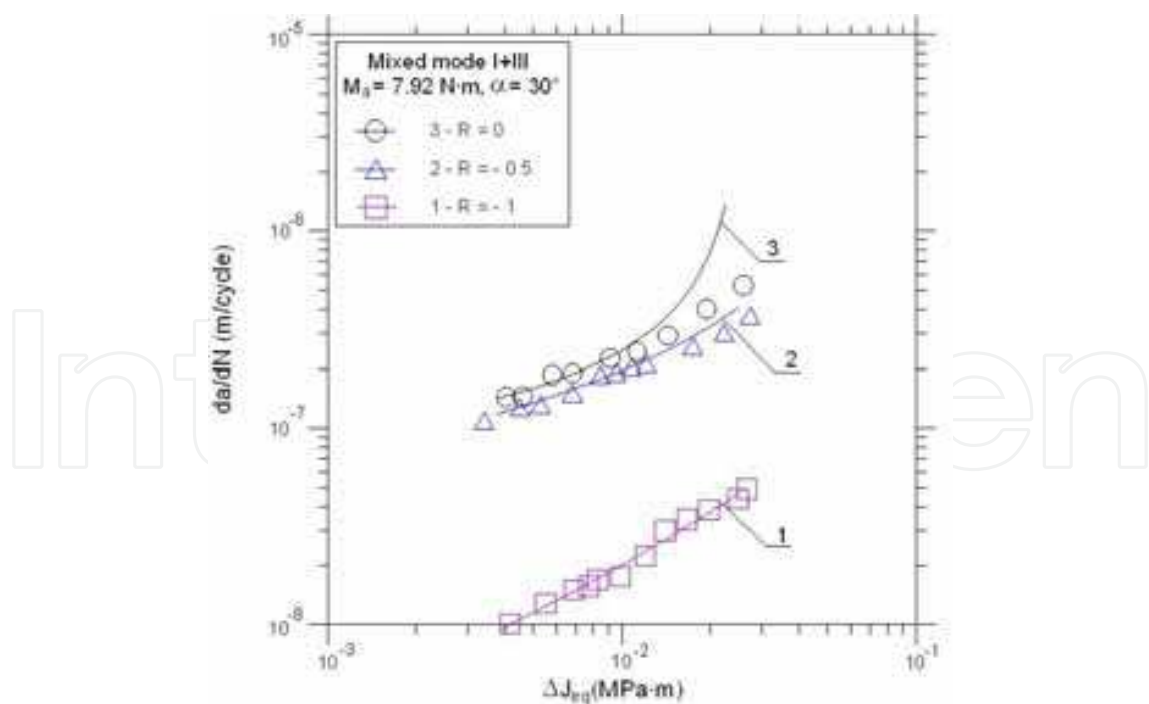


Fig. 17. Comparison of the experimental results with calculated ones according to Eq. (8) for $\alpha = 30^\circ$ and mixed mode I+ III

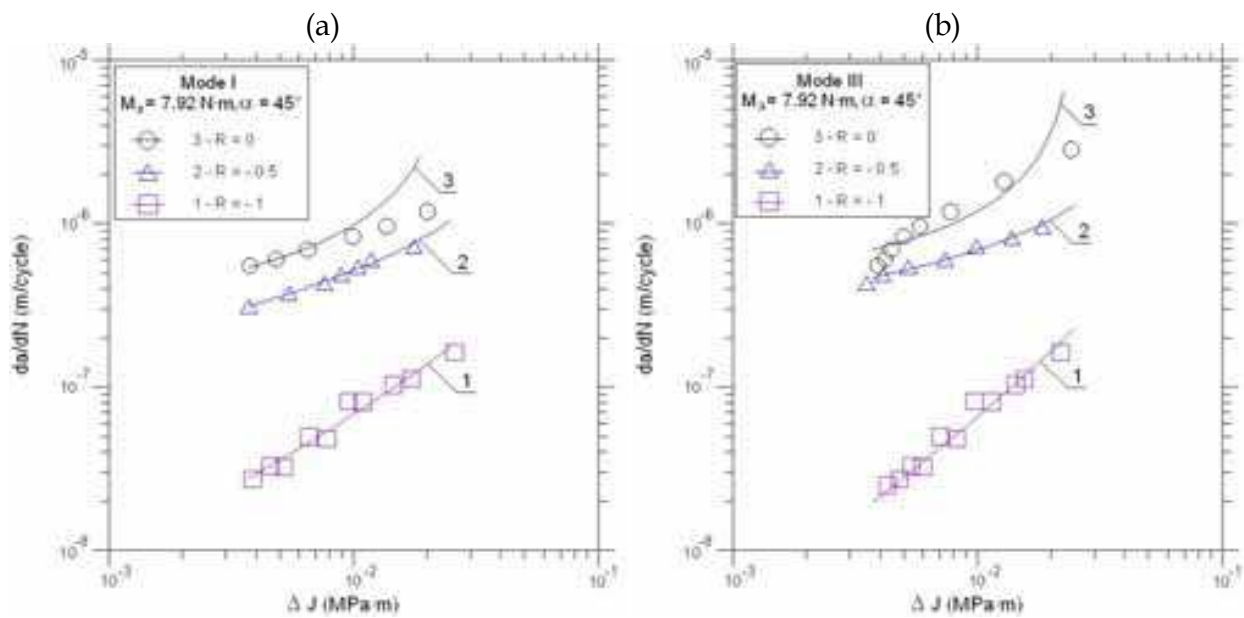


Fig. 18. Comparison of the experimental results with calculated ones according to Eq. (8) for $\alpha = 45^\circ$ and: (a) mode I, (b) mode III

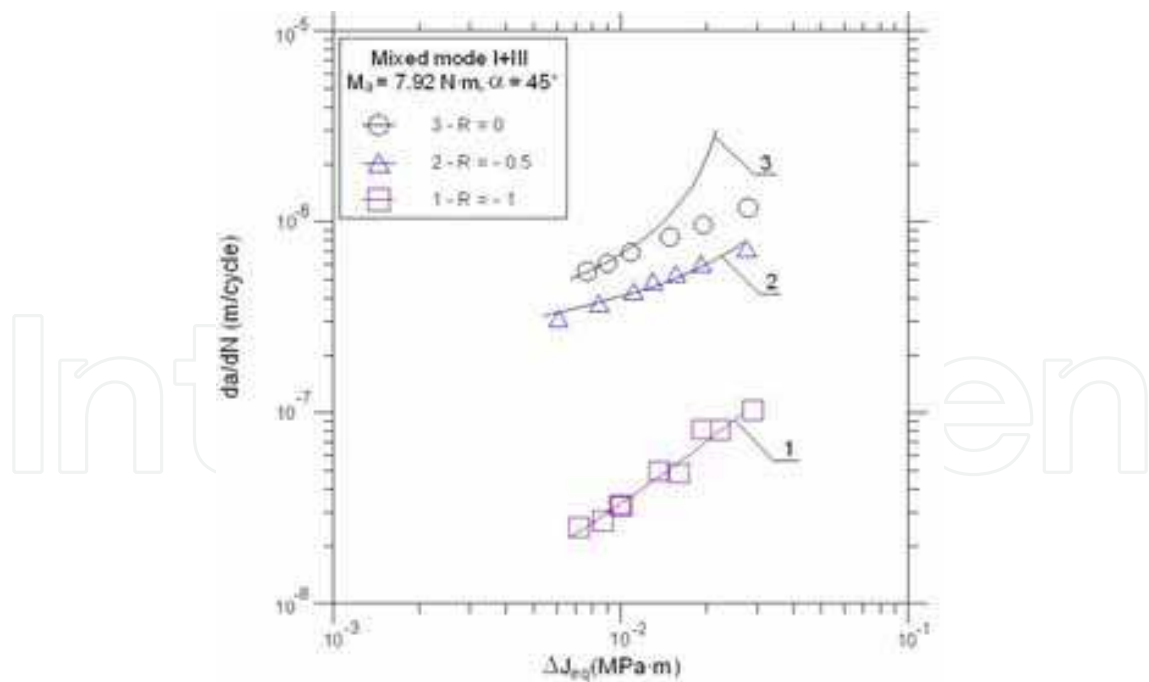


Fig. 19. Comparison of the experimental results with calculated ones according to Eq. (8) for $\alpha = 45^\circ$ and mixed mode I+ III

For $R = -1$ and $\alpha = 45^\circ$ (Fig. 18), a higher crack growth rate was found for mode I to $da/dN = 8 \cdot 10^{-8}$ m/cycle above that value mode III was dominating together with increase of the material plasticity. This behaviour is due to the decrease of normal stresses and increasing shear stresses. The test results presented in Figs. 16 - 21 were described with the empirical formula (8). Eq. (8) is valid for mode I and mode III as well as for mixed mode I+III loading.

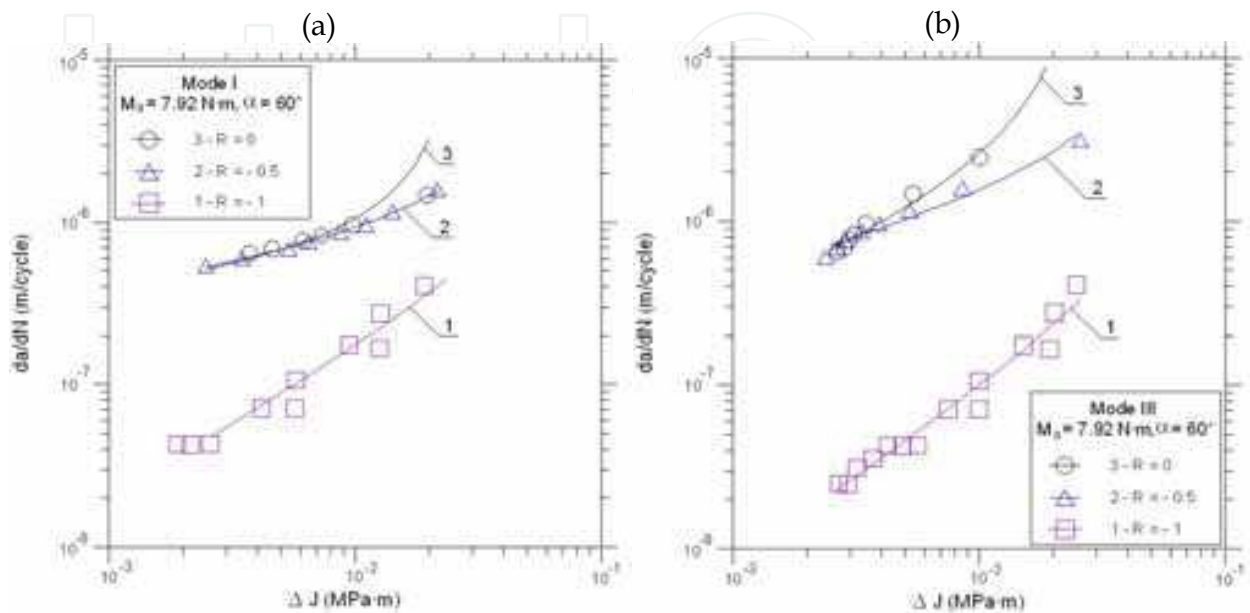


Fig. 20. Comparison of the experimental results with calculated ones according to Eq. (8) for $\alpha = 60^\circ$ and: (a) mode I, (b) mode III

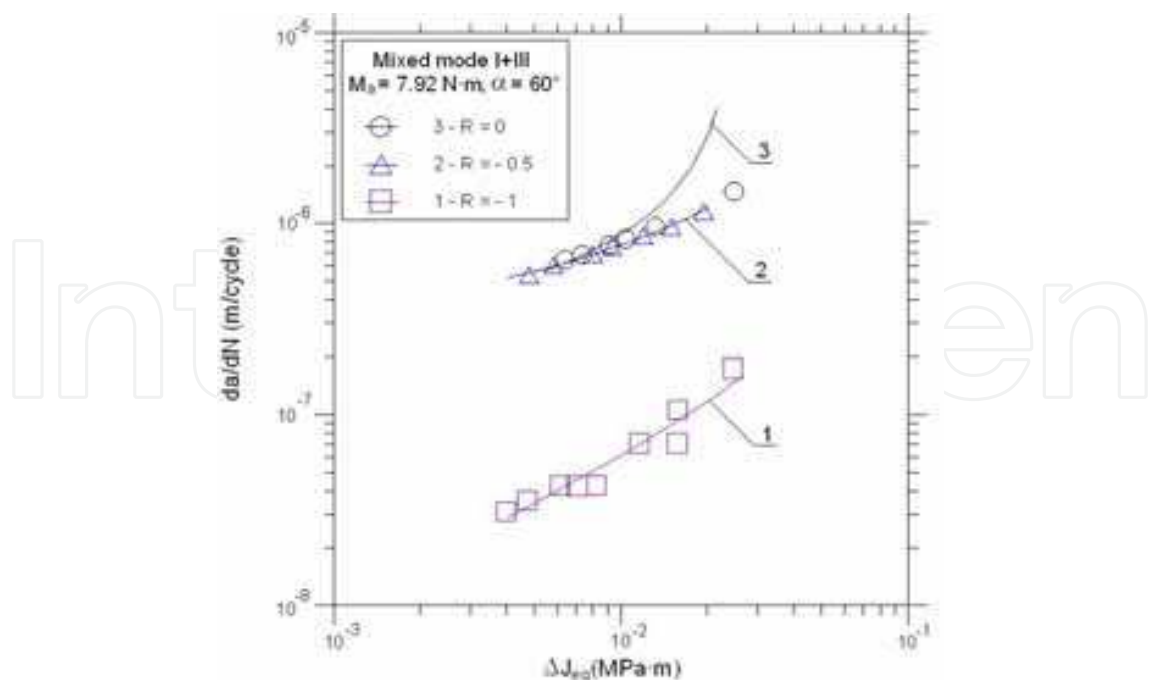


Fig. 21. Comparison of the experimental results with calculated ones according to Eq. (8) for $\alpha = 60^\circ$ and mixed mode I+ III

The applied empirical formula (8) including ΔJ parameter gives good results in the description of fatigue crack growth rate. Surfaces of fatigue fractures were analysed (magnification 13x) in order to determine directions of the normal stress (mode I) and the shear stress (mode III). In the cases of mixed mode I+III and $\alpha = 30^\circ, 45^\circ$ and 60° , principal directions of stresses change their positions. During tests under bending with torsion (Fig. 12) and $\alpha = 30^\circ$, the fatigue crack growth proceeded at the average angle $\alpha_1 = 25^\circ$, and under $\alpha = 45^\circ$ - at the angle $\alpha_1 = 33^\circ - 37^\circ$, and under $\alpha = 60^\circ$ - at the angle $\alpha_1 = 40^\circ - 43^\circ$ to the cross section of the specimens.

The empirical coefficients B and n occurring in Eq. (8) were calculated with the least square method and they were shown in Table 5. The coefficients take different values for pure bending and pure torsion. It means that B and n are not dependent on a kind of the material only. The test results for cyclic bending with torsion include the error not exceeding 20% at the significance level $\alpha = 0.05$ for the correlation coefficients r_w given in Table 5.

Figs.	Graphs	B MPa·m ² /cycle	n	r _w
16a	1	1.46·10 ⁻⁷	0.86	0.99
	2	0.73·10 ⁻⁷	0.40	0.99
	3	0.31·10 ⁻⁷	0.35	0.99
16b	1	5.52·10 ⁻⁷	0.98	0.98
	2	1.35·10 ⁻⁷	0.43	0.99
	3	0.80·10 ⁻⁷	0.49	0.99
17	1	0.56·10 ⁻⁷	0.73	0.99
	2	0.62·10 ⁻⁷	0.40	0.99
	3	0.15·10 ⁻⁷	0.24	0.98
18a	1	3.23·10 ⁻⁷	0.85	0.99
	2	1.42·10 ⁻⁷	0.38	0.99
	3	0.57·10 ⁻⁷	0.28	0.98
18b	1	1.35·10 ⁻⁶	1.17	0.99
	2	1.22·10 ⁻⁷	0.28	0.99
	3	0.50·10 ⁻⁷	0.21	0.97
19	1	2.23·10 ⁻⁷	0.93	0.98
	2	0.58·10 ⁻⁷	0.23	0.99
	3	0.41·10 ⁻⁷	0.29	0.98
20a	1	1.10·10 ⁻⁶	0.91	0.98
	2	1.88·10 ⁻⁷	0.31	0.99
	3	0.51·10 ⁻⁷	0.24	0.99
20b	1	1.20·10 ⁻⁶	1.05	0.98
	2	6.22·10 ⁻⁷	0.46	0.99
	3	1.08·10 ⁻⁶	0.71	0.99
21	1	2.03·10 ⁻⁷	0.77	0.98
	2	1.59·10 ⁻⁷	0.32	0.99
	3	0.57·10 ⁻⁷	0.31	0.98

Table 5. Coefficients B and n in Eq. (8) and correlation coefficients r_w for the curves shown in Figs. 16 - 21

The test results indicate that the ΔJ parameter concept may be applied to fatigue problems in linear-elastic or nonlinear elastic-plastic fracture mechanics. The trends described in the chapter were confirmed for various loads and three load ratios. Because of its properties the ΔJ parameter may appear the main energetic criterion for fatigue crack growth characterizing the crack tip strain field for cyclic loading. Directions of future research will focus on fatigue cracks growth under non-proportional and random loads.

4. Conclusion

The presented results of the fatigue crack growth rate in AlCu4Mg1 aluminium alloy subjected to cyclic bending and proportional bending with torsion loading under different load ratio allow to formulate the following conclusions:

1. On the specimen fractures we can observe usually transcrystalline cracks through grains of the phase α , but also cracks along the grain boundaries can be noticed.
2. It has been shown that the applied parameter ΔJ as compared with the parameter ΔK for different load ratios R is better for description of fatigue crack growth rate.
3. Increase of the angle α determining a ratio of the torsional moment to the bending moment and load ratio causes increase of the fatigue crack growth rate.
4. In the case of separation of the mixed mode I+III loading into the pure mode I and mode III, for $\alpha = 30^\circ, 45^\circ, 60^\circ$ and $R = -0.5, 0$ the fatigue crack growth rate is higher for mode III compared with mode I under the same value ΔJ .

5. Acknowledgements

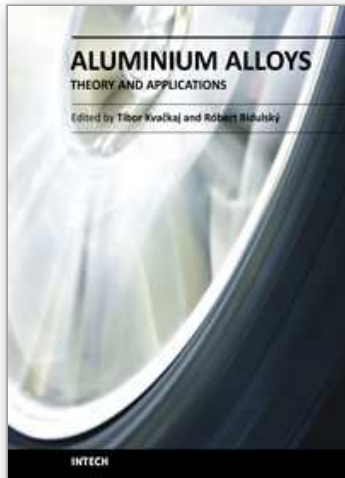
This work was supported by the National Centre for Research and Development, Contract No. N R03 0065 06.

6. References

- ASTM E1820-99, (1999). Standard test method for measurement of fracture toughness, *Annual Book of American Society for Testing and Materials Standards*, Vol. 03.01, ISBN 0-8031-2712-X, Philadelphia
- Chell, G.G. & Girvan, E. (1978). An experimental technique for fast fracture testing in mixed mode, *Int. J. Fracture*, Vol. 14, No. 2, pp. R81-R84
- Chung, K.H. & Yang, W.H. (2003). Mixed mode fatigue crack growth in aluminium plates with composite patches, *Int. J of Fatigue*, Vol. 25, No. 4, pp. 325-333, ISSN 0142-1123
- Döring, R.; Hoffmeyer, J.; Seeger, T. & Vormwald, M. (2006). Short fatigue crack growth nonproportional multiaxial elastic-plastic strains, *Int. J of Fatigue*, Vol. 28, No. 9, pp. 972-982, ISSN 0142-1123
- Harris, D.O. (1967). Stress intensity factors for hollow circumferentially notched round bars, *Jurnal Bas. Engng.*, Vol. 89, No. 49, pp. 121-126
- Kocańda, S. & Kozubowski, J. (1974). Ermüdungsbrüche von ausscheidungen in aluminiumlegierungen, *Zeitschrift f. Metallkunde* 6, s. 453-456
- Pokluda, A. J. (2004). Intrinsic thresholds of long fatigue cracks, *Proceedings of XX Symposium Fatigue and Fracture Mechanics*, pp. 327-337, ISBN 83-89334-06-2, Bydgoszcz-Pieczyska, April 2004, Akademia Techniczno-Rolnicza, Pieczyska

- Rozumek, D. (2005). Fatigue crack growth rate in aluminium alloy including mixed mode I and III, *Journal of Theoretical and Applied Mechanics*, Vol. 43, No. 4, pp. 731-743, ISSN 1429-2955
- Rozumek, D. (2005). J-integral in description of fatigue crack growth rate, *The Archive of Mechanical Engineering*, Vol. LII, No. 1, pp. 51-62, ISSN 0004-0738
- Rozumek, D. (2009). Mixed mode fatigue cracks of constructional materials, Studies and Monographs No. 241, Opole University of Technology, ISSN 1429-6063, Opole, (in Polish)
- Rozumek, D. & Macha, E. (2006). A description of fatigue crack growth in elastic-plastic materials under proportional bending with torsion, Opole University of Technology, ISBN 83-88492-08-X, Opole, (in Polish)
- Rozumek, D. & Macha, E. (2009). J-integral in the description of fatigue crack growth rate induced by different ratios of torsion to bending loading in AlCu4Mg1, *Materialwissenschaft und Werkstofftechnik*, Vol. 40, No. 10, pp. 743-749, ISSN 1521-4052
- Rozumek, D. & Marciniak, Z. (2010). Fatigue crack growth of specimens with rectangular cross-sections under out-of-phase bending and torsional loading, *Proceedings of the XV International Colloquium Mechanical Fatigue of Metals (XV-ICMFM)*, pp. 45-45 and CD, ps 8, ISBN 978-83-60691-83-0, Opole, September 2010, Opole University of Technology, Opole
- Thum, A.; Petersen, C. & Swenson, O. (1960). Verformung, Spannung und Kerbwirkung, *VDI*, Düsseldorf

IntechOpen



Aluminium Alloys, Theory and Applications

Edited by Prof. Tibor Kvackaj

ISBN 978-953-307-244-9

Hard cover, 400 pages

Publisher InTech

Published online 04, February, 2011

Published in print edition February, 2011

The present book enhances in detail the scope and objective of various developmental activities of the aluminium alloys. A lot of research on aluminium alloys has been performed. Currently, the research efforts are connected to the relatively new methods and processes. We hope that people new to the aluminium alloys investigation will find this book to be of assistance for the industry and university fields enabling them to keep up-to-date with the latest developments in aluminium alloys research.

How to reference

In order to correctly reference this scholarly work, feel free to copy and paste the following:

Dariusz Rozumek and Ewald Macha (2011). Crack Growth in AlCu4Mg1 Alloy under Combined Cyclic Bending and Torsion, Aluminium Alloys, Theory and Applications, Prof. Tibor Kvackaj (Ed.), ISBN: 978-953-307-244-9, InTech, Available from: <http://www.intechopen.com/books/aluminium-alloys-theory-and-applications/crack-growth-in-alcu4mg1-alloy-under-combined-cyclic-bending-and-torsion>

INTECH
open science | open minds

InTech Europe

University Campus STeP Ri
Slavka Krautzeka 83/A
51000 Rijeka, Croatia
Phone: +385 (51) 770 447
Fax: +385 (51) 686 166
www.intechopen.com

InTech China

Unit 405, Office Block, Hotel Equatorial Shanghai
No.65, Yan An Road (West), Shanghai, 200040, China
中国上海市延安西路65号上海国际贵都大饭店办公楼405单元
Phone: +86-21-62489820
Fax: +86-21-62489821

© 2011 The Author(s). Licensee IntechOpen. This chapter is distributed under the terms of the [Creative Commons Attribution-NonCommercial-ShareAlike-3.0 License](#), which permits use, distribution and reproduction for non-commercial purposes, provided the original is properly cited and derivative works building on this content are distributed under the same license.

IntechOpen

IntechOpen